

## Formation of complex bacterial colonies via self-generated vortices

András Czirók,<sup>1</sup> Eshel Ben-Jacob,<sup>2</sup> Inon Cohen,<sup>2</sup> and Tamás Vicsek<sup>1,3</sup>

<sup>1</sup>*Department of Atomic Physics, Eötvös University, Puskin u. 5-7, 1088 Budapest, Hungary*

<sup>2</sup>*School of Physics, Tel-Aviv University, 69978 Tel-Aviv, Israel*

<sup>3</sup>*Institute for Technical Physics, P.O. Box 76, 1325 Budapest, Hungary*

(Received 23 October 1995; revised manuscript received 29 March 1996)

Depending on the environmental conditions bacterial colonies growing on agar surfaces can exhibit *complex colony formation* and various types of *collective motion*. Experimental results are presented concerning the hydrodynamics (vortices, migration of bacteria in clusters) and colony formation of a morphotype of *Bacillus subtilis*. Some of these features are not specific to this morphotype but also have been observed in several other bacterial strains, suggesting the presence of universal effects. A simple model of self-propelled particles is proposed, which is capable of describing the hydrodynamics on the intermediate level, including the experimentally observed rotating disks of bacteria. The colony formation is captured by a complex generic model taking into account nutrient diffusion, reproduction, and sporulation of bacteria, extracellular slime deposition, chemoregulation, and inhomogeneous population. Our model also sheds light on some possible biological benefits of this “multicellular behavior.” [S1063-651X(96)04408-X]

PACS number(s): 87.10.+e, 87.22.-q, 05.60+w

### I. INTRODUCTION

Recently great efforts have been devoted to the understanding of biological regulation pathways in various organisms, and in many cases the corresponding mechanisms have been identified at the molecular level. However, facing a complex network of regulation systems on the intermediate scale of the interactions among groups of cells, we usually lack powerful biological experimental methods. The study of *bacterial colonies* can yield interesting insight into the interactions in such self-organized structures, since these colonies represent perhaps the *simplest* biological systems showing *collective behavior* [1–6]. In this case we can hope that the interactions are still simple enough to be captured by mathematical models and exploring the collective behavior needs feasible computational power. Indeed, the study of bacterial colonies and mathematical models incorporating the corresponding physical knowledge and biological data [7–16] has revealed the importance of various effects, such as diffusional instabilities (see, e.g., Ref. [17,18]) in the control of colony formation.

In this paper we focus on a fascinating phenomenon including the development of *complex patterns* and various types of *collective motion* in bacterial colonies. In particular, several observations have been made on the rotation of disk shaped aggregates, migration of groups of bacteria, or their peculiar motion along ring shaped trajectories. Although such types of motion have commonly been associated with *Bacillus circulans*, similar phenomena have been seen in colonies of *Archangium violanceum*, *Chondromyces apiculatus*, *Clostridium tetani* [19], and recently in our experiments with a morphotype [20] of *Bacillus subtilis*. Such collective rotation of many bacteria has represented a long standing question without any explanation so far. Here we propose a solution to this puzzle using models based on the assumption that the motion of bacteria is determined by a few relevant effects.

Understanding this self-organized motion of micro-

organisms provides an important clue into the mechanisms of their communication and survival strategies. We believe that the experimentally observed behavior is a response to the hostile environment such as diffusion limited growth conditions and/or hard agar substrate. In general, as growth conditions worsen, a more complex global structure is observed together with a higher microlevel organization. Efficient adaptation requires self-organization on all levels. To achieve this, bacteria developed sophisticated communication channels on all levels: from direct (by contact) bacterium-bacterium physical interaction, through indirect (long-range) chemical signaling, to genetic communication via exchange of genetic material.

As the phenomena studied are extremely rich, we cannot expect to understand them by building as simple algorithmic models as diffusion-limited aggregation [21] or the Eden model [22]. However, we can study *minimal models* with the smallest possible number of interactions and parameters to mimic the experimental behavior for *various external conditions* [14,15,23]. Exploring the parameter space one can test whether the proposed interactions are sufficient to describe the observed phenomena. This approach is an application of the methods common in statistical physics [24–26] to biological systems consisting of many, relatively simple units exhibiting collective behavior.

The paper is organized as follows: A summary of our experimental results is presented in Sec. II. In Sec. III we introduce a model of self-propelled particles explaining the observed “exotic” hydrodynamics to some extent on the mesoscopic (intermediate) scale. In Sec. IV this model will be refined to a biologically more plausible model including chemotaxis signaling. In Sec. V our model is further expanded to describe colony formation on the macroscopic level.

### II. EXPERIMENTAL OBSERVATIONS

Bacterial colonies grown under favorable (standard) growth conditions usually do not exhibit a high level of or-

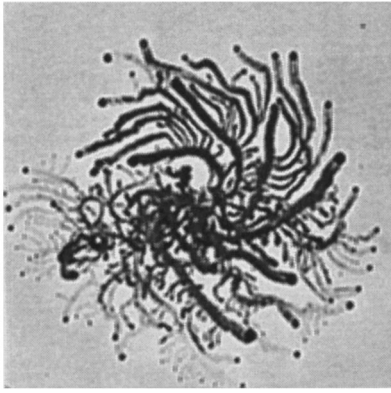


FIG. 1. A typical colony formed by the *vortex* morphotype. Each branch is formed by a rotating droplet of many bacteria moving together in a correlated manner at the tips of the branches.

ganization. However, recent experimental results indicate that under certain hostile environmental conditions (e.g., when the available amount of nutrients is limited by diffusion, or the hard agar surface inhibits the motion of bacteria) the colony may behave as a “multicellular organism” [2]: *cell differentiation* appears, and *long-range information transmission* occurs via diffusing chemicals.

In our experiments we investigated a morphotype (named *vortex*) derived from the strain *Bacillus subtilis* 168 [9]. The colonies were grown in standard (88 mm) plastic Petri dishes, on hard agar substrates containing peptone (Bacto-Peptone; Difco) as nutrient source. Thus, the concentration of agar and peptone played the role of control parameters. The colonies were incubated in a closed incubator at a temperature of  $35 \pm 1.5$  °C and 30% humidity. Growth was started with a  $5 \mu\text{l}$  droplet (containing about  $10^5$  bacteria) inoculation placed at the center of the Petri dishes. Microscopic observations were performed using a bright field optical microscope (Olympus BH2-UMA) with ultralong range objectives allowing a total magnification of  $500\times$ . As no immersion liquid was needed, these long working distance objectives enabled us to observe the undisturbed motion of the micro-organisms *on the agar surface*. For more details of the experiments see, e.g., Refs. [9] and [14].

In Fig. 1 an example of the colonies formed by the *Vortex* morphotype is shown. The colonies spread via leading droplets (the darker dots), leaving a clearly observable trail filled with bacteria behind. Each droplet consists of many bacteria rotating around a common center (hence the name vortex) at typical velocities of  $10 \mu\text{m/s}$ . Depending on the growth conditions and the location inside of the colony, the number of bacteria in a single vortex can vary from a couple of hundred to many thousand, and the vortex can consist of both single and multiple layers of bacteria. Usually, the “pioneering” droplets are larger, while the smaller ones fill the empty areas left behind by the advancing front. Within a single colony, both clockwise and anticlockwise rotating vortices can be observed.

These patterns are formed on *rich* ( $\approx 5$  g/l peptone) and *hard* ( $\approx 20$  g/l agar) media, where the colony formation of the other morphotypes [9,13,14] is strongly hindered as the individual bacteria can hardly move. In our case the motion is performed in a collective manner: bacteria form groups and the motion of individual cells shows a very high level of

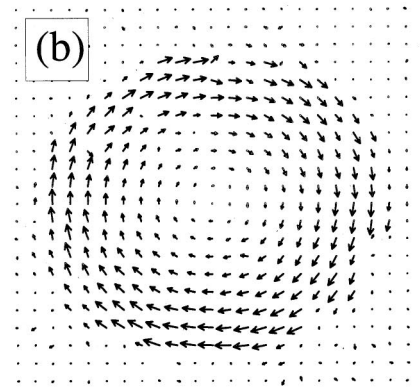
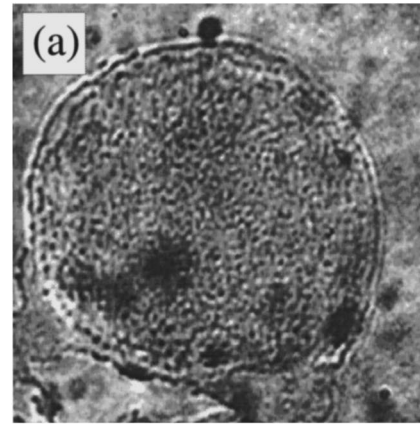


FIG. 2. Bright field micrograph of a single rotating droplet with a magnification of  $500\times$  (a) and the corresponding velocity field obtained by digitizing our video recordings (b).

correlation. A typical flow field of a leading vortex [Fig. 2(a)] is shown in Fig. 2(b), which has been obtained by digitizing the video micrograph recordings and numerically analyzing the data (see Appendix A for details).

The above, and numerous other similar observations, indicate the presence of such unusual flow patterns even in relatively simple biological systems. As we show in the next section, this is due to the fact that unlike most abiotic objects, living organisms are *self-propelled*: they can transform energy gained from food into mechanical energy, which allows them to change their position.

### III. SELF-PROPELLED PARTICLES

The motion of bacteria is determined by various effects such as the driving force of their flagella, the viscosity of the surrounding fluid (extracellular slime), and the elastic and chemical properties of the cell-cell contact. Many of these local interactions can be incorporated into a *phenomenological model*, where bacteria are represented as moving and interacting particles.

#### A. Description of the model

In the simplest model of collective bacterial movement, each particle’s velocity is set to a fixed magnitude  $v$ , result-

ing from the driving force of the flagellar motor of the bacteria. The interaction changes only the direction of motion: the particles tend to align their orientation to the local average velocity [27]. This effect can be originated (at least in part) from geometrical constraints: steric repulsion between rodlike particles, similar to the interactions in nematic liquid crystals, see, e.g., Ref. [28].

Thus, let us consider a system of particles moving on the plane with an (average) density  $\varrho$ . Each particle is characterized by its location  $\vec{x}_i(t)$  and orientation  $\vartheta_i(t)$  indicating the direction of motion:  $\vartheta_i(t) = \Phi[\vec{v}_i(t)]$ , where the function  $\Phi(\vec{r})$  gives the angle between the argument vector and a selected direction (e.g.,  $x$  coordinate axis). The time evolution of the orientation is given by the following equation describing the *coalignment interaction* of the  $i$ th particle:

$$\frac{d\vartheta_i}{dt} = \frac{1}{\tau} [\langle \vartheta(t) \rangle_{i,\epsilon} - \vartheta_i(t)] + \zeta, \quad (1)$$

where  $\zeta$  represents an uncorrelated noise (e.g., accounting for the Brownian character of the motion of the bacteria) and  $\langle \vartheta(t) \rangle_{i,\epsilon}$  denotes the average direction of motion of the particles in the neighborhood (within a radius  $\epsilon$ ) of the  $i$ th particle as

$$\langle \vartheta(t) \rangle_{i,\epsilon} = \Phi \left( \sum_{\substack{j \\ |\vec{x}_j - \vec{x}_i| \leq \epsilon}} \vec{v}_j(t) \right). \quad (2)$$

The relaxation time  $\tau$  in Eq. (1) is related to the bacterial length to width ratio: for longer bacteria the interaction is more pronounced.

In this system the total momentum is not conserved, as can be demonstrated by the interaction of two particles, where the total momentum is increasing as they tend to move along parallel trajectories. Thus, the flow field emerging in the model (and also in bacterial colonies) can considerably differ from the usual behavior of fluids.

To explore this behavior, we performed Monte Carlo simulations. Instead of Eq. (1) a simpler, time-discretized expression was used that was valid if the rotational relaxation process is fast compared to the change of the locations ( $\tau \ll v^{-1}/\sqrt{\varrho}$ ):

$$\vartheta_i(t + \Delta t) = \langle \vartheta(t) \rangle_{i,\epsilon} + \zeta, \quad (3)$$

where the noise  $\zeta$  is a random variable with uniform distribution in the interval  $[-\eta/2, \eta/2]$ . The positions of the particles were updated using Eulerian discretization,

$$\vec{x}_i(t + \Delta t) = \vec{x}_i(t) + \vec{v}_i(t)\Delta t. \quad (4)$$

The simulations were performed in a square of size  $L \times L$  and a periodic boundary condition was applied. As the initial condition the position and the direction of motion of the particles were distributed randomly.

### B. Collective migration

In the various simulations [27,29] two control parameters ( $\eta$  and  $\varrho$ ) were changed, while  $v$  was kept constant in the  $v \ll \epsilon/\Delta t$  regime. For small  $\eta$  and high density an *ordered*

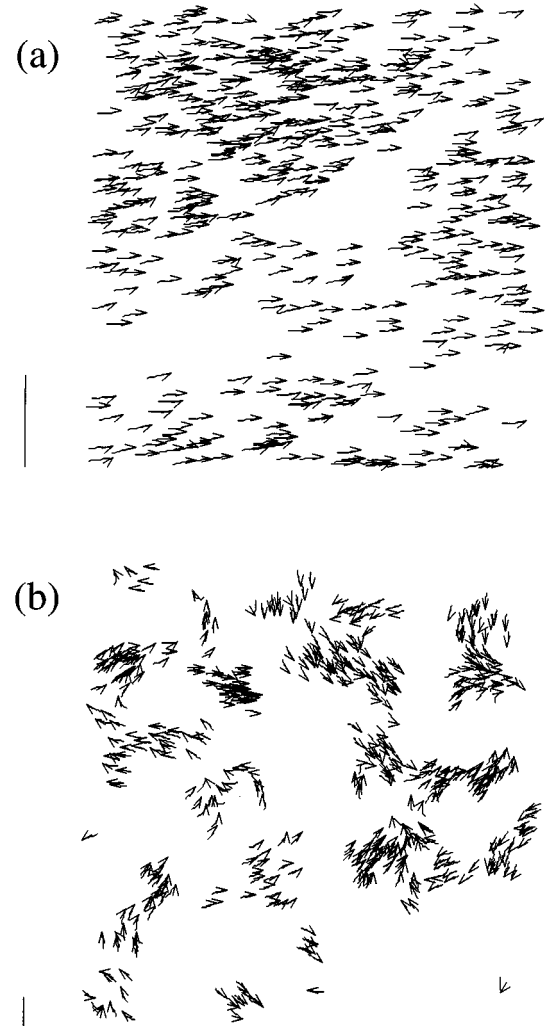


FIG. 3. The velocities of the self-propelled particles are displayed for various values of density and noise. The *actual velocity* of a particle is indicated by a small arrow, while its trajectory for the last 20 time steps is shown by a short continuous curve. The number of particles was  $N=300$  in each case and the velocity  $v$  was set to equal to 0.04. For comparison, the range of the interaction ( $\epsilon=1$ ) is displayed as a bar. At high densities and small noise ( $L=5$  and  $\eta=0.1$ ) the motion becomes ordered (a). For small densities and noise ( $L=25$  and  $\eta=0.1$ ) the particles tend to form groups moving coherently in random directions (b).

*phase* emerges [Fig. 3(a)]: all particles move in the same direction over length scales much longer than the range of the interaction ( $\epsilon$ ).

At low density and small noise amplitude several clusters are formed [Fig. 3(b)]. Such a cluster is held together due to the parallel velocities of the particles in the group. The collision of the clusters usually creates a larger cluster, which later breaks into parts due to the inherent weak randomness of the velocities.

Increasing the amplitude of the noise for a fixed density, at a critical value of  $\eta$  the net flow disappears following a transition that is reminiscent of *second-order phase transitions* in equilibrium physical systems [30,31] (Fig. 4). Thus our model is a transport related, nonequilibrium analog of the ferromagnetic type of model: The Hamiltonian tending to

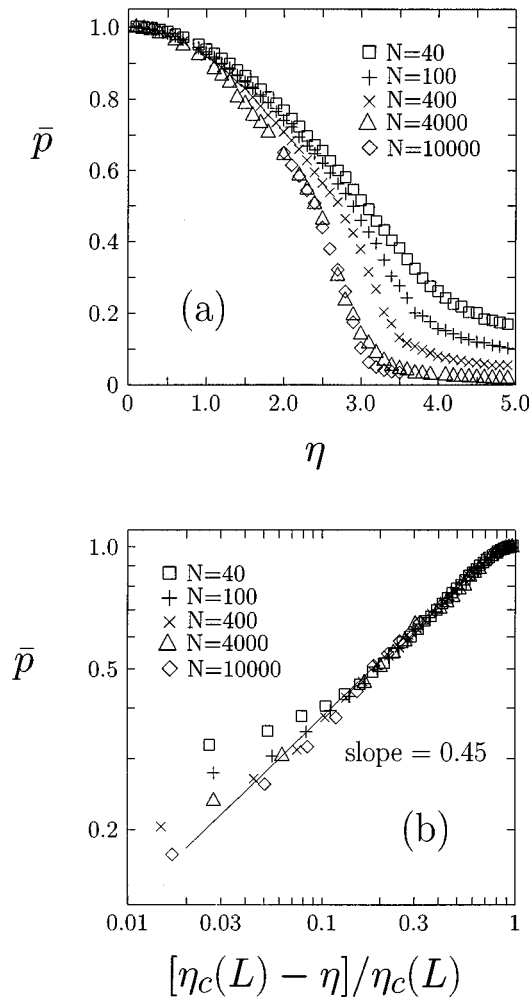


FIG. 4. (a) The total momentum of the system  $\bar{p}$  versus the noise  $\eta$  in systems of various sizes with a fixed density  $\rho$ . The symbols denote the following.  $\square$  :  $N=40$ ,  $L=3.1$ ;  $+$  :  $N=100$ ,  $L=5$ ;  $\times$  :  $N=400$ ,  $L=10$ ;  $\triangle$  :  $N=4000$ ,  $L=31.6$ .  $\diamond$  :  $N=10\,000$ ,  $L=50$ . (b) Dependence of  $\bar{p}$  on the reduced noise  $[\eta - \eta_c(L)]/\eta_c(L)$  on a double logarithmic plot. The slope of the line fitted to the data indicates critical scaling behavior.

align the spins in the same direction in the case of equilibrium ferromagnets is replaced by the rule of aligning the direction of motion of the particles. The (normalized) magnitude of the total momentum of the system can be considered as an *order parameter* and the critical noise  $\eta_c$  as an analog of the *critical temperature*. For more details about this transition see Ref. [27].

### C. Hard-core repulsion

To gain additional insight into the properties of the model, we carried out the numerical simulations of a slightly modified system: The boundary conditions were changed to *reflective circular walls*, and to avoid singular behavior at the boundaries (aggregation of particles in a narrow zone), a *short range “hard-core” repulsion* was also incorporated into the model. If the distance between the bacteria is smaller than  $\epsilon^*$  (the size of a single bacterium), they repel each other

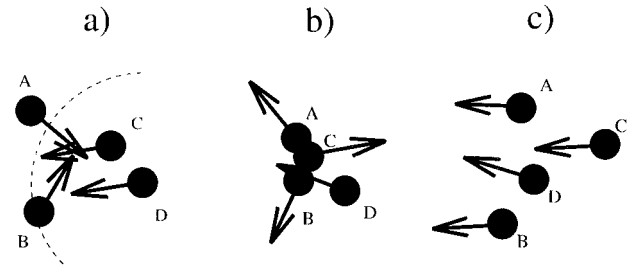


FIG. 5. Schematic illustration of the model with both hard-core interaction and ferromagneticlike coupling of the velocities. The figure shows the position and velocity (arrows) of the particles at time  $t$  (a),  $t + \Delta t$  (b), and  $t + 2\Delta t$  (c). The range of the hard-core repulsion ( $\epsilon^*$ ) is represented as a filled circle. The dashed circle in (a) indicates the range of velocity coupling ( $\epsilon$ ) for particle D. In the collision at time  $t + \Delta t$  A, B, and C particles repel each other, while the new velocity of particle D was determined by the average direction of motion of B, C, and D. At time  $t + 2\Delta t$  no collision occurs, each particle is moving approximately with the local average velocity.

and the direction of their motion will be given by the following expression instead of Eq. (3):

$$\vartheta_i(t + \Delta t) = \Phi \left( - \sum_{\substack{j \neq i \\ |\vec{x}_j - \vec{x}_i| < \epsilon^*}} \mathbf{N}(\vec{x}_j(t) - \vec{x}_i(t)) \right), \quad (5)$$

where  $\mathbf{N}(\vec{u})$  denotes  $\vec{u}/|\vec{u}|$ ; see Fig. 5.

In agreement with the results of very recent molecular dynamical simulations of related self-propelled systems [25,26], in the high density, low noise regime correlated rotation can be observed (Fig. 6). The direction of the rotation is selected by spontaneous symmetry breaking, thus both clockwise and anticlockwise spinning “vortices” emerge.

As this example shows, appropriate boundary conditions can lead to spontaneous rotation in a system of locally interacting self-propelled particles. However, in bacterial colonies numerous vortices can be observed far from the boundary of the colony, thus the confinement of the bacteria (which was an externally posed boundary in the above example) must be the result of some interaction of the organisms. To incorpo-

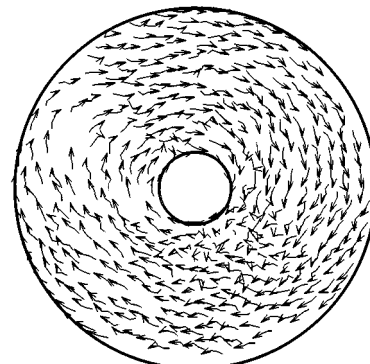


FIG. 6. Stationary state of the model represented in Fig. 5. The boundary conditions are reflective walls ( $R=10$ ,  $\epsilon^*=0.1$ ,  $\epsilon=1$ ,  $\eta=0.1$ ).

rate such an interaction into the model, first we refine this simple model of collective bacterial motion.

#### IV. VORTEX FORMATION

Although locally the bacteria move with a uniform velocity, on a larger scale one can clearly observe groups moving with various velocities. The velocity field measurements of a rotating vortex also show that the simple representation of the bacteria as particles with a fixed velocity must be refined.

We replace our former assumption of constant velocity with an assumption of constant (resultant) propulsion force  $F$  being parallel to the actual velocity. Now the magnitude of the velocity is determined via the balance of this driving force on one hand and friction with the substrate and a drag force produced by the mean velocity of the surrounding bacteria on the other hand. Moreover, the interaction among bacteria still includes a hard-core force, which is assumed to be proportional to  $-\nabla\varrho$ , where  $\varrho$  denotes the local density (number of particles in a unit area). In large (multilayer) vortices this expression can be originated from the hydrodynamic term  $\nabla p$  assuming that the mechanical pressure is proportional to the number of layers, hence to the density. In small (single-layer) vortices this term may be considered as an approximation for the hard-core interaction. Combining these terms we obtain the following equation of motion for the  $i$ th particle:

$$\frac{d\vec{v}_i}{dt} = \mu[\langle\vec{v}\rangle_{i,\epsilon} - \vec{v}_i] - \nu\vec{v}_i + F\frac{\vec{v}_i}{v_i} - \kappa\vec{\nabla}\varrho + \vec{\zeta}. \quad (6)$$

The  $\mu$ ,  $\nu$ , and  $\kappa$  coefficients are parameters of the model, which characterize the various types of bacteria. In principle  $\mu$ ,  $\nu$ , and  $F$  depend also on the local amount of extracellular slime deposited.

What is needed to turn a collective migration into spontaneously formed vortices? In Sec. III we showed that geometrical constraints of circular reflecting boundaries lead to a circular collective movement. This result suggests that a radial inward force can lead to vortex formation. Motivated by the demonstrated role of chemoattractants in other colonies [4,6,14,32] and our expectation about universality [32], we propose that an emission of a kind of chemoattractant can provide the needed effect.

##### A. Collective ‘‘chemotaxis’’

Usually chemotaxis [33] means that the motion of the organisms is influenced by chemical fields, e.g., bacteria in a liquid culture perform a biased random walk towards the nutrients [34]. In this paper we use the words ‘‘chemotaxis’’ and ‘‘chemoattractant’’ in a broad sense, the particular response we consider can result from ‘‘passive’’ physical forces, such as surface tension or the changing efficiency of the flagellar motors as a function of the amount and quality of the extracellular slime deposited. In contrast, in the usual (active) chemotactic response specific biochemical machinery—membrane receptors and intracellular regulatory pathways—are involved.

Since collectively migrating bacteria do not tumble on the agar surface, they clearly had to develop a different mechanism of chemotactic response. Here we propose that in this

case the chemotaxis is a response of a group of bacteria (often called raft or cohorse [1]): We assume that the individual bacteria slightly change the propulsion force of their flagella depending on the local concentration of the attractant, which results in a torque acting on the group. This effect creates a local vorticity in the following manner, if we assume for simplicity that the total driving force (hence the magnitude of the velocity) of the group does not change.

Let us consider a raft (group of bacteria) moving in a concentration field  $c_A$ . Supposing that the raft is held together by intercellular bonds, we treat it as a rigid body of size  $d$ . In a linear approximation the velocity difference at the opposite sides of the raft is proportional to the component of  $\nabla c_A$  being orthogonal to the velocity:

$$\Delta v \sim \frac{d}{v} |\vec{v} \times \vec{\nabla} c_A|. \quad (7)$$

The change in the direction of the velocity ( $\Delta\vartheta$ ) during an infinitesimal time interval  $\Delta t$  can be expressed as  $\Delta v/d$ , thus the term describing attractive chemotactic response in the equation of motion can be written in the form of

$$\frac{d\vec{v}}{dt} \sim -\frac{1}{v} \vec{v} \times (\vec{v} \times \vec{\nabla} c_A). \quad (8)$$

To indicate the special nature of this chemotactic response we denote it as *rotor chemotaxis* in the following. Including this chemotaxis term (using the ‘‘sensitivity’’ coefficient  $\chi_A$ ) to the full equation of motion yields

$$\begin{aligned} \frac{d\vec{v}_i}{dt} = & \mu[\langle\vec{v}\rangle_{i,\epsilon} - \vec{v}_i] - \nu\vec{v}_i + F\frac{\vec{v}_i}{v_i} - \kappa\vec{\nabla}\varrho \\ & - \frac{\chi_A}{v_i} \vec{v}_i \times (\vec{v}_i \times \vec{\nabla} c_A) + \vec{\zeta}. \end{aligned} \quad (9)$$

The time evolution of the chemoattractant field is described by the following equation if we neglect the convective transport caused by the motion of bacteria:

$$\frac{\partial c_A}{\partial t} = D_A \nabla^2 c_A + \Gamma_A \varrho - \lambda_A c_A. \quad (10)$$

The first and the third terms represent the diffusion and the constant rate ( $\lambda_A$ ) decay, respectively, while the second (source) term assumes that all bacteria are under stress conditions and continuously produce the chemoattractant with a rate of  $\Gamma_A$ . This is a useful assumption if we investigate the formation of a single vortex, but must be refined when we also intend to describe the colony morphogenesis.

##### B. Numerical results

The simulation of the above model was carried out through the numerical integration of Eqs. (9) and (10). To discretize the fields  $c_A$  and  $\varrho$  a *triangular lattice* was defined with lattice vectors  $\vec{e}_1, \vec{e}_2, \dots, \vec{e}_6$  ( $|\vec{e}_i| = a$ , see Fig. 7).  $\varrho$  was calculated as the number of particles in the lattice cells. The differential operators were calculated as

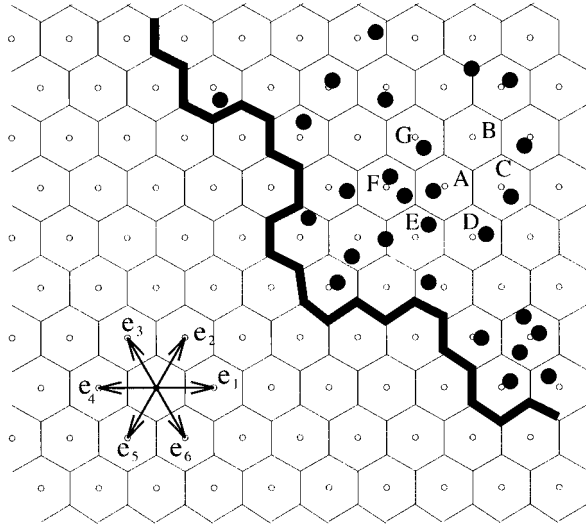


FIG. 7. Schematic illustration of the chemoregulated model. The diffusing chemoattractant is calculated in the grid points of a triangular lattice (open circles). The lattice vectors are denoted by  $\vec{e}_1, \vec{e}_2, \dots, \vec{e}_6$ . The particles (filled circles) move off lattice, and are reflected at the boundary (thick line). To calculate the average flow  $\langle \vec{v} \rangle_{i,\epsilon}$  for the particle in lattice cell A, we average over all particle in the cells A–G.

$$\partial_x c(\vec{r}) \approx \frac{c(\vec{r} + \vec{e}_1) - c(\vec{r} + \vec{e}_4)}{2a}, \quad (11)$$

$$\partial_y c(\vec{r}) \approx \frac{c(\vec{r} + \vec{e}_1) + c(\vec{r} + \vec{e}_2) - c(\vec{r} + \vec{e}_5) - c(\vec{r} + \vec{e}_6)}{2\sqrt{3}a}, \quad (12)$$

$$\nabla^2 c(\vec{r}) \approx \frac{2}{3} \frac{\sum_{i=1}^6 c(\vec{r} + \vec{e}_i) - 6c(\vec{r})}{a^2}. \quad (13)$$

The particles moved off lattice, but for computational efficiency the  $\langle \vec{v} \rangle_{i,\epsilon}$  local average velocity was approximated by averaging over all particles in the lattice cell containing the  $i$ th particle, and also over the particles occupying the neighboring cells. This is consistent with the choice of  $\epsilon \approx 3a/2$ . Particles could move in an area bounded by reflective boundaries. However, in contrast with the simulations described in Sec. III, here we obtained vortex formation on a *smaller scale* than the system size, thus in this case the boundaries had negligible effects. Again, as an initial condition we applied  $c_A = 0$  and random configuration of the particles.

The *positive feedback* of the attractive chemotaxis breaks the originally homogeneous spatial distribution of the particles and creates dense aggregates: If a fluctuation increases the density locally, then the emission of chemoattractants (being proportional to  $\varrho$ ) is also increased, and this increased  $\vec{\nabla} c_A$  attracts even more particles to the aggregate. As a consequence of the *coalignment* term, rotation develops in a spontaneously selected direction. In such an aggregate the difference of the  $\vec{\nabla} \varrho$  term and the attractive force of chemotaxis provides the appropriate centripetal acceleration. Typi-

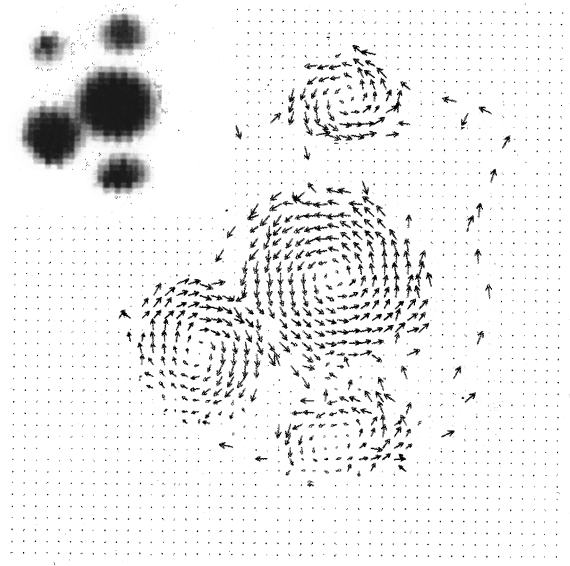


FIG. 8. A typical result of the chemoregulated model for vortex formation. The positive feedback of the chemoattractant breaks the originally homogeneous density and aggregates with high density are created. The flow field is represented by arrows of a magnitude proportional with the local velocity. The inset shows the concentration distribution of the chemoattractant ( $\mu = 0.1$ ,  $\nu = 0.1$ ,  $F = 0.3$ ,  $\kappa = 0.1$ ,  $\chi_A = 0.2$ ,  $\eta = 0.2$ ,  $D_A = 0.1$ ,  $\lambda_A = 0.01$ ).

cal vortices formed in our model are shown in Fig. 8, being in good agreement with experimental observations (Fig. 2). For different parameter values the model yields rotating rings reported also in experiments (Fig. 9). The qualitative results discussed here turned out to be robust against changing the form of Eq. (9) until a cohesive force with coalignment interaction is represented.

## V. COLONY FORMATION

The model introduced in the previous section is able to describe and explain many experimentally observed features on the intermediate scale, such as collective migration of groups, and formation of rotating dense aggregates in which the direction of the spinning was selected by spontaneous symmetry breaking. However, that model is far from being complete, since it cannot describe colony formation on the macroscopic level, which is certainly a needed step in understanding the possible (evolutionary) benefits of this behavior. To expand the model to describe colony morphogenesis, further details must be considered: extracellular slime influencing the motion of the organisms, and nutrient diffusion and consumption determining the growth rate of the colony and additional chemical regulation of the movement of the individual vortices.

### A. Extracellular fluid

According to microscopic observations, there is a well defined *boundary* of the colony dividing the substrate into parts where bacteria can and cannot move. In order to migrate on a solid agar surface bacteria have to “wet” the surface either by drawing water from the substrate or by producing some extracellular slime. This assumption is sup-

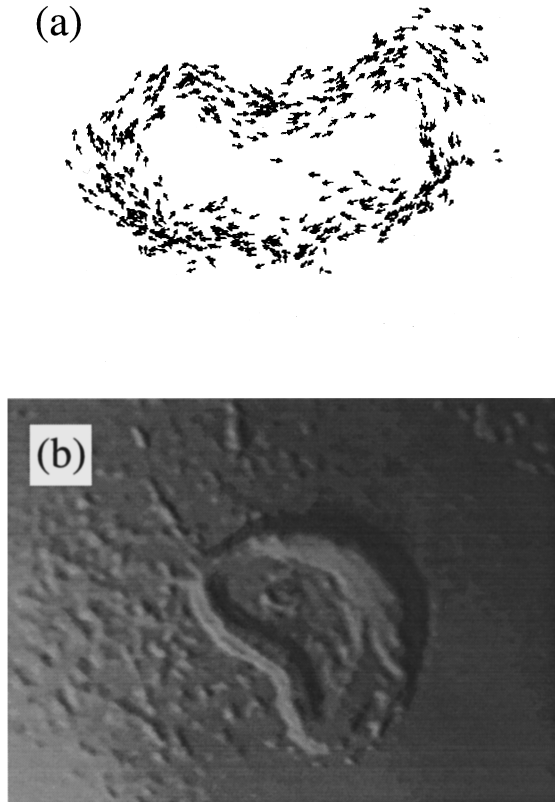


FIG. 9. In the same model as shown in Fig. 8, but for a different value of the parameter  $\mu$  (providing stronger velocity-velocity interaction,  $\mu=0.3$ ), rotating rings develop in the simulations (a). This phenomenon was also reported in Ref. [19] (b).

ported by many reports on swarmer strains such as *Proteus* [35,36] and also by our microscopic observations [14]: the boundary of the colony propagates as bacteria deposit lubrication fluid at “unoccupied” positions.

We will assume in the model that particles can move only at sites where the deposited amount of extracellular slime [denoted by  $w(\vec{r})$ ] is larger than a threshold value  $W$ : if they encounter a drop of  $w$  to  $w(\vec{r}') < W$  during the step to the lattice cell  $\vec{r}'$ , they will be reflected from the boundary separating the two cells. To ensure the displacement of the boundary we assume that with each attempt to move into an unoccupied site, the particles deposit the amount of fluid they carried ( $s_i$ ) to the outer side of the boundary into the unoccupied lattice cell. More precisely, bacteria deposit fluid if the surface is dry:  $w(\vec{r}') < W'$ , where the threshold  $W'$  is larger than  $W$ . The detailed equations (including production and decay) are presented in Appendix B.

### B. Nutrient consumption

So far, the investigated hydrodynamical phenomena were fast compared to the multiplication of bacteria. When studying the colony formation, however, we cannot ignore nutrient consumption, multiplication, and sporulation. To describe these effects, we adopt the model introduced in Ref. [14] with slight modifications of the equations. We denote by  $c(\vec{r})$  the concentration of the *growth limiting nutrient* in the medium, and by  $E_i$  the metabolic state (“*internal energy*”)

of the particles. We consider  $E_i$  as a generic parameter of the cell-cycle (referring approximately to the cell volume in the case of real bacteria), which affects the activity of the particles as described below.

The particles lose “energy” (e.g., due to dissipative metabolic processes) at a constant rate  $e$ . To increase  $E_i$  the model bacteria consume nutrients at a rate proportional to the available concentration and independent of the number of bacteria in the surroundings. This approximation is valid for small nutrient concentrations and bacterium density.

When there is not enough food for an interval of time causing  $E_i$  to drop to zero, the bacteria become stationary (e.g., *sporulate*). At this stage of the model sporulation is irreversible: there is no recovery of activity if the nutrient concentration is increased. As the spores do not move, they are characterized by their density (number of spores in a lattice cell)  $\varrho_s$  only.

When nutrients are available in a sufficient amount,  $E_i$  increases and when it reaches some threshold  $E^*$ , the model particle *divides into two*. During the division process a given amount of energy ( $e^*$ ) is dissipated and the remaining energy is shared equally among the two offspring. Thus the time evolution of  $E_i$  is given by

$$\frac{dE_i}{dt} = r_c c(x_i) - e - \frac{E^* + e^*}{2} \delta(E_i - E^*). \quad (14)$$

The nutrient is diffusing and consumed by the bacteria:

$$\frac{\partial c}{\partial t} = D \nabla^2 c - r_c c \varrho. \quad (15)$$

Equation (15) is discretized and solved on the same lattice as  $c_A$  and  $w$ .

### C. Response to chemorepellent

Developed colonies of the vortex morphotype exhibit fascinating patterns, which shows complex self-organization of the vortices. Even the most complex patterns are not random and inoculations under the same growth conditions lead to reproducible observations. Clearly, a high level of regulatory mechanisms must be operative during the colony development, which must be capable of moving each vortex as a single unit. Keeping again our notion of universality (the existence of similar phenomena in other bacterial strains) we propose that long range repulsive chemotaxis is the regulating mechanism.

Each of the stationary particles (or alternatively, bacteria that have been exposed to low level of nutrients) produces a diffusing repellent chemical at a fixed rate of  $\Gamma_R$ ,

$$\frac{\partial c_R}{\partial t} = D_R \nabla^2 c_R + \Gamma_R \varrho_s - \lambda_R c_R, \quad (16)$$

where  $c_R$  and  $\varrho_s$  denote the concentration of the repellent and the density of the stationary bacteria, respectively, while  $\lambda_R$  gives the decay rate. The effect of the chemical on the movement of the bacteria is given by the rotor chemotaxis (8) term coupled with the coefficient  $\chi_R$  as

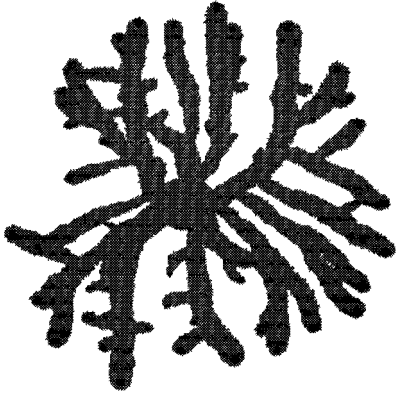


FIG. 10. Typical colony obtained from numerical simulations of the model incorporating nutrient diffusion, reproduction, and sporulation of bacteria, chemotactic regulation, velocity-velocity interaction, and extracellular fluid deposition. The simulation is performed in a  $600 \times 600$  system with ca. 100 000 particles. In excellent agreement with the experimental observations, the colony grows via rotating droplets at the tips of the branches. Smaller vortices also emerge inside the colony, sometimes giving rise to a new side branch.

$$\begin{aligned} \frac{d\vec{v}_i}{dt} = & \mu[\langle \vec{v} \rangle_{i,\epsilon} - \vec{v}_i] - \nu \vec{v}_i + F \frac{\vec{v}_i}{v_i} - \kappa \vec{\nabla}(\varrho + \varrho_s) \\ & - \frac{1}{v_i} \vec{v}_i \times [\vec{v}_i \times (\chi_A \vec{\nabla} c_A - \chi_R \vec{\nabla} c_R)] + \vec{\zeta}. \end{aligned} \quad (17)$$

To get realistic results from the simulations, only one additional feature is needed: in the present stage of the model the particles cannot leave the aggregates, in contrast with the experiments where some (usually inactive but not sporulated) bacteria are always left behind the vortices. In the framework of the model this means that *not all the bacteria have the same sensitivity to the chemoregulators*, some of them must respond less to the gradients (e.g., because their receptors are saturated or being in an inactive phase). To model this we assumed that in each time step particles “turn off” the receptors with a probability of  $P_0$ , and “turn on” with a probability of  $P_1$ . In this case sometimes groups of particles leave the aggregates, move behind and form a smaller new vortex, which may create a new side branch (see Fig. 10). The equations governing the full model are summarized in Appendix B.

#### D. Increase of fitness

To understand the possible benefits of vortex formation, let us investigate a vortex in a colony grown under diffusion-limited conditions. As beyond the vortex (inside the colony) the nutrient concentration is rather small (this plausible assumption is supported also by the numerical results of our model), vortices are exposed to a nutrient field with a strong gradient.

Our calculations (Appendix C) show that in this case the rotation of the aggregates reduces the *energy dissipation rate* of the reproductive and sporulation processes, thus the whole aggregate of bacteria can spend more energy to enhance the speed of the propagation (e.g., by producing more lubrication

fluid). Under diffusion-limited conditions the faster propagation increases the inflow of nutrients (hence the available amount of energy), thus increasing the fitness of the colony.

The strategy reducing the rate of multiplication and using the energy for colonizing surfaces is not a unique feature of vortex forming bacteria. In the case of swarmer strains similar behavior was reported [1]: the differentiated swarmer cells are specialized to expand the colony, and many of their metabolic pathways (including the multiplication processes) are repressed.

Another possible benefit suggested by our model that can balance the energy spent on maintaining the rotation is the more efficient transport of the extracellular fluid inside the vortices.

## VI. CONCLUSIONS

A generic phenomenological model for the collective motion of bacteria on a solid agar surface has been presented based on a ferromagneticlike coupling of the velocities of self-propelled particles. Numerical results showed that this model can be completed with different biologically motivated interactions to capture many of the experimentally observed features in bacterial colonies, where self-organized transport develops with spontaneous breaking of the rotational or translational symmetry.

Based on this dynamics, a complex model has been constructed to explain both the hydrodynamics on the mesoscopic level and the colony formation on the macroscopic level. The minimal set of *microscopic* interactions we had to consider is the following: ferromagneticlike coupling of the velocities and a hard-core interaction (e.g., due to geometrical constraints); response to a “chemoattractant” to hold the groups of bacteria together; nutrient consumption, multiplication, and sporulation; extracellular slime production and deposition; chemoregulation to control the motion of rafts and vortices; and “diversity” of the population (parameters providing that the particles are not completely equivalent). Thus, we cannot identify a single dominant effect being responsible for the observed behavior, but we have to deal with a set of interactions, each of them having the same level of importance. The schematic representation of the generic features of the model is given in Fig. 11.

The question of the *robustness* of the approach presented arises in a natural way. First, the experimental data for various external conditions and organization levels (ranging from the possible microscopic interactions through the mesoscopic flow field to features of the movement to colony formation) yield strict constraints for the model. Moreover, some of the generic features such as nutrient consumption, multiplication, sporulation, and chemoregulation are successfully adopted in other models as well. Second, a broad range of parameters yields the same behavior (we did not have to perform a specific “fine tuning” to obtain the results presented) with similar insensitivity to the specific functional form of the interactions. Thus, our results suggest the potential power of the generic modeling approach in understanding complex biological systems.

One of the main messages of our work is that it is possible to interpret the experimentally observed complex (sometimes

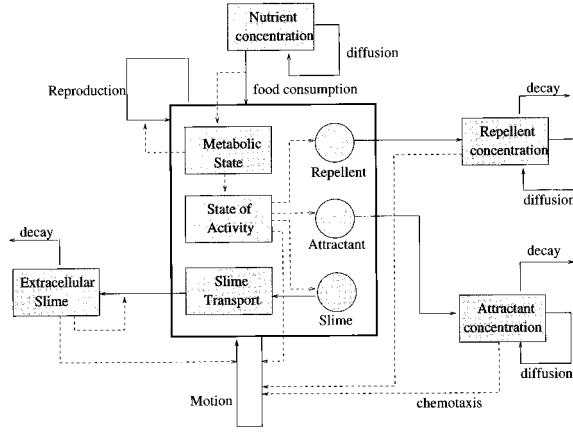


FIG. 11. Schematic flow diagram of the model. The solid and dashed arrows indicate material transfer and regulatory connections, respectively. The central rectangle represents the particles with internal parameters (filled boxes) and production of various chemicals (filled circles). The chemical concentration fields describe the environment of the particle.

puzzling) behavior of the ensemble of bacteria through many-particle-type simulation incorporating realistic rules. In our opinion, our approach is novel in the sense that the more traditional simulations either (i) are based on much simpler assumptions (aggregation, cellular automata, etc.) or (ii) involve biological details, but are numerically very different and their application to cases with complicated environment or geometry is not feasible.

#### ACKNOWLEDGMENTS

We have benefited from conversations with Z. Csahók, K. Márialigeti, and O. Shochet. We thank I. Brainis for technical assistance. This work was supported by the Hungarian Research Foundation Grant (OTKA) No. T4439 and No. F017246, by a grant from the German-Israeli Foundation for Scientific Research and Development, and by the Program for Alternative Thinking at Tel-Aviv University.

#### APPENDIX A: IMAGE PROCESSING

To determine the velocity field of the colonies using the consecutive frames of a video recording the following procedure was performed: First, to reduce the digitization noise, we applied a simple high-frequency filter (smoothing) on the images as

$$h_t(i, j) \rightarrow \frac{1}{9} \sum_{-1 \leq m, n \leq 1} h_t(i+m, j+n), \quad (\text{A1})$$

where we denoted the gray scale level of pixel  $(i, j)$  on the frame corresponding to time  $t$  by  $h_t(i, j)$ .

To reconstruct the flow field from the digitized video records, we tracked various small details on the consecutive frames. Let us consider a small image of linear size  $2L$ , which was centered at  $(i_0, j_0)$  at time  $t$  and moved to the position  $(i, j)$  on the frame corresponding to  $t + \Delta t$ . In this case the velocity  $\vec{v}_t(i_0, j_0)$  at  $(i_0, j_0)$  is given approximately by  $[(i - i_0)/\Delta t, (j - j_0)/\Delta t]$ . To locate the selected image on the new frame, we scan a window of linear size  $2L$  over the

new frame and calculate its overlap  $d_L$  with the original image for each possible position  $(i, j)$  as

$$d_L^2(i_0, j_0, i, j) = \sum_{|m, n| \leq L} [h_t(i_0 + m, j_0 + n) - h_{t+\Delta t}(i + m, j + n)]^2. \quad (\text{A2})$$

The new location is identified as the position that gives maximal overlap.

The efficiency of the method described above is sensitive to both  $\Delta t$  and  $L$ . On one hand  $L$  and  $\Delta t$  should be small enough to reduce the effects of the flow inhomogeneity and the rotation of the image. On the other hand with increasing  $L$  the traced image contains more information allowing easier identification. The typical value of  $L$  we used is 20.

#### APPENDIX B: SUMMARY OF THE MODEL

Variables describing the state of a model bacterium are as follows:  $\vec{x}_i$ , location;  $\vec{v}_i$ , velocity;  $E_i$ , ‘‘internal energy’’;  $s_i$ , amount of lubrication fluid carried;  $\Omega_i$ , state of activity.  $\Omega_i = 0, 1$  represents states differing in the sensitivity to chemotaxis, while  $\Omega_i = 2$  represents an inactive bacterium;  $\vec{\zeta}$ , white noise with an amplitude of  $\eta$ .

Fields describing the environment are as follows:  $c(\vec{r})$ , concentration of the growth limiting nutrient;  $c_A(\vec{r})$ , concentration of the emitted chemoattractant;  $c_R(\vec{r})$ , concentration of the chemorepellent;  $\varrho(\vec{r})$ , density of the bacteria;  $\varrho_s(\vec{r})$ , density of the spores;  $w(\vec{r})$ , amount of extracellular fluid deposited.

Equations governing the dynamics of these variables are as follows:

$$\Omega_i(t+1) = \begin{cases} \Omega_i(t) & \text{with probability } 1 - P_{\Omega_i(t)} \\ 1 - \Omega_i(t) & \text{with probability } P_{\Omega_i(t)} \\ 2 & \text{if } E_i(t) < 0, \end{cases} \quad (\text{B1})$$

$$\vec{x}_i(t + \Delta t) = \begin{cases} \vec{x}_i(t) + \vec{v}_i \Delta t & \text{if } w(\vec{\xi}_i) > W \\ \vec{x}_i(t) - \vec{v}_i \Delta t & \text{if } w(\vec{\xi}_i) \leq W, \end{cases} \quad (\text{B2})$$

$$\begin{aligned} \frac{\Delta \vec{v}_i}{\Delta t} = & \mu[\langle \vec{v} \rangle_{i, \epsilon} - \vec{v}_i] - \nu \vec{v}_i + F \frac{\vec{v}_i}{v_i} - \kappa \vec{\nabla}(\varrho + \varrho_s) \\ & - \frac{1}{v_i} \vec{v}_i \times [\vec{v}_i \times (\chi_A \nabla c_A - \chi_R \nabla c_R)] + \vec{\zeta}, \end{aligned} \quad (\text{B3})$$

$$\frac{\Delta E_i}{\Delta t} = r_c c - e - \frac{E_i + e^*}{2} \Theta(E_i - E^*), \quad (\text{B4})$$

$$\frac{\Delta s_i}{\Delta t} = \Gamma_s - T(\vec{\xi}_i) \frac{s_i}{\sum_j \delta_{\vec{\xi}_i, \vec{\xi}_j} s_j} - \lambda_s s_i, \quad (\text{B5})$$

$$T(\vec{r}) = \min \left( \sum_i \delta_{\vec{r}, \vec{\xi}_i} s_i, W' - w(\vec{r}) \right), \quad (\text{B6})$$

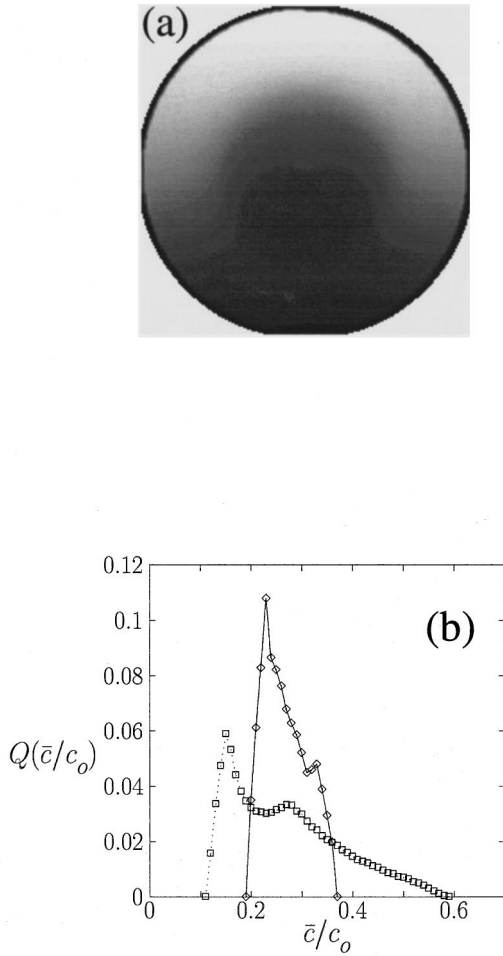


FIG. 12. Numerically calculated concentration field of the nutrient in the neighborhood of a disk shaped group of bacteria (a) and the calculated  $Q(\bar{c})$  density function (b). In the case of the rotating vortex (dashed line) the distribution is sharper yielding a reduced dissipation of energy in comparison with the nonrotating case (solid line).

$$\frac{\Delta c}{\Delta t} = D \nabla^2 c - r_c c \varrho, \quad (\text{B7})$$

$$\frac{\Delta c_R}{\Delta t} = D_R \nabla^2 c_R - \lambda_R c_R + \Gamma_R \varrho_s, \quad (\text{B8})$$

$$\frac{\Delta c_A}{\Delta t} = D_A \nabla^2 c_A - \lambda_A c_A + \Gamma_A \varrho, \quad (\text{B9})$$

$$\frac{\Delta w(\vec{r})}{\Delta t} = T(\vec{r}) - \lambda_s w(\vec{r}), \quad (\text{B10})$$

where  $\Theta(x)$  denotes the Heaviside function:  $\Theta(x)=0$  for  $x \leq 0$  and  $\Theta(x)=1$  for  $x > 0$ , and  $\vec{\xi}_i$  denotes the lattice cell containing  $\vec{x}_i + \vec{v}_i \Delta t$ .

Coupling and rate coefficients are as follows:  $D, D_A, D_R$ , diffusion coefficients;  $\lambda_A, \lambda_R, \lambda_s$ , decay coefficients;  $r_c$ , rate of nutrient consumption;  $\Gamma_A, \Gamma_R, \Gamma_s$ , emission rate of chemicals;  $\mu, \nu$ , friction coefficients;  $\chi_A, \chi_R$ , sensitivity to the chemoregulators;  $F$ , driving force of the

bacteria;  $e$ , minimal rate of “internal energy” consumption;  $e^*$ , energy dissipation at division;  $E^*$ , threshold for division;  $W, W'$ , thresholds for extracellular fluid deposition; and  $P_0, P_1$ , transition probabilities between states 0 and 1.

### APPENDIX C: EFFECTS OF VORTEX FORMATION ON MULTIPLICATION

To mimic a vortex aggregate in the diffusion-limited colony, let us consider a disk of bacteria with a fixed radius of  $R$  and fixed density  $\varrho_0$  as

$$\varrho(r, \phi) = \varrho_0 \Theta(R - r), \quad (\text{C1})$$

and a diffusing nutrient that is consumed by the bacteria according to Eq. (16). The presence of a nonzero gradient is forced by the boundary condition for the nutrient concentration  $c$ :

$$c(R', \phi) = c_0 \frac{\sin \phi + 1}{2}, \quad (\text{C2})$$

where  $R' > R$  is the boundary of the field. If no bacteria were present, this boundary condition would yield a stationary field with a constant gradient:

$$c(r, \phi) = c_0 \frac{r \sin \phi + R'}{2R'}. \quad (\text{C3})$$

Now let us focus on the reproduction of the bacteria. According to our model, bacteria divide when the “internal energy” accumulated exceeds  $(E^* + e^*)/2$ , the amount of energy loss at division. This condition determines  $T_i$ , the time elapsed between two consecutive multiplication of the  $i$ th bacterium in an implicit manner,

$$\frac{E^* + e^*}{2} = c_r \int_0^{T_i} c(\vec{x}_i(t)) dt - T_i e = T_i (r_c \bar{c}_i - e), \quad (\text{C4})$$

where the overbar denotes averaging over the path of a given particle during its “cell cycle”:  $\bar{c}_i = 1/T_i \int_0^{T_i} c[\vec{x}_i(t)] dt$ . Expressing the growth rate  $\lambda_i = 1/T_i$  yields

$$\lambda_i = \frac{2}{E^* + e^*} (r_c \bar{c}_i - e). \quad (\text{C5})$$

If the rotation is fast compared to  $T$  (being the case in both the experiments and the simulations) then  $\bar{c}_i \approx \int c(\vec{r}_i, \phi) d\phi$ , where the position of the particle is expressed in polar coordinates:  $x_i = (r_i, \phi_i)$ . We should compare this situation with the case when rotation is missing:  $\bar{c}_i \approx c(\vec{r}_i, \phi_i)$ .

Let us denote by  $P(\lambda) d\lambda$  the probability of finding a particle with a growth rate in the interval  $[\lambda, \lambda + d\lambda]$ . This probability density can be calculated by relaxing numerically Eq. (16) with the boundary conditions (C2). If  $c(r, \phi)$  is known, then  $Q(\bar{c})$  (the density distribution of  $\bar{c}$ ) can be related to  $P(\lambda)$  as

$$P(\lambda)d\lambda = Q\left(\frac{2}{E^*+e^*}(r_c\bar{c}_i - e)\right) \frac{2r_c}{E^*+e^*}d\bar{c}. \quad (C6)$$

Figure 12(a) shows the calculated stationary concentration field, and Fig. 12(b) shows the corresponding probability density  $Q(\bar{c})$  for both the rotating and nonrotating cases. As we could expect, when the vortex is rotating the distribution is sharper (there are less starving and fast reproducing bacteria) due to the averaging. This also means that a larger  $e$  (and a reduced total growth rate) can be maintained for the bacteria forming the rotating disk.

The energy inflow ( $\Sigma_i \bar{c}_i$ ) is determined by the diffusion of the nutrient, hence being the same in both cases considered. When the vortex is rotating the *rate of energy dissipation by multiplication*  $e^* \int_0^\infty P(\lambda)d\lambda = e^* \int_{e/r_c}^\infty Q(\bar{c})d\bar{c}$  is reduced: bacteria can spend more energy to enhance the speed of the propagation of the group (e.g., by producing more lubrication fluid). The faster propagation—which was not captured in this simple calculation—increases the inflow of nutrients (hence the available amount of energy), thus increasing the fitness of the colony.

- 
- [1] C. Allison and C. Hughes, *Sci. Prog.* **75**, 403 (1991).  
 [2] J.A. Shapiro, *Sci. Am.* **256**, 82 (1988).  
 [3] J.A. Shapiro and D. Trubatch, *Physica D* **49**, 214 (1991).  
 [4] E.O. Budrene and H.C. Berg, *Nature* **349**, 630 (1991).  
 [5] Y. Blat and M. Eisenbach, *J. Bact.* **177**, 1683 (1995).  
 [6] E.O. Budrene and H.C. Berg, *Nature* **376**, 49 (1995).  
 [7] H. Fujikawa and M. Matsushita, *J. Phys. Soc. Jpn.* **58**, 3875 (1989).  
 [8] M. Matsushita and H. Fujikawa, *Physica A* **168**, 498 (1990).  
 [9] E. Ben-Jacob, H. Shmueli, O. Shochet, and A. Tenenbaum, *Physica A* **187**, 378 (1992).  
 [10] M. Matsushita, J. Wakita, and T. Matsuyama, in *Proceedings of the NATO Advanced Research Workshop on Spatio-Temporal Patterns in Nonequilibrium Complex Systems, Santa Fe, 1993* (Addison-Wesley, Reading, 1995).  
 [11] T. Matsuyama, R.M. Harshey, and M. Matsushita, *Fractals* **1**, 302 (1993).  
 [12] T. Vicsek, A. Czirók, O. Shochet, and E. Ben-Jacob, in *Proceedings of the NATO Advanced Research Workshop on Spatio-Temporal Patterns in Nonequilibrium Complex Systems, Santa Fe, 1993* (Ref. [10]).  
 [13] E. Ben-Jacob, A. Tenenbaum, O. Shochet, and O. Avidan, *Physica A* **202**, 1 (1994).  
 [14] E. Ben-Jacob, O. Shochet, A. Tenenbaum, I. Cohen, A. Czirók, and T. Vicsek, *Nature* **386**, 46 (1994); *Fractals* **2**, 1 (1994).  
 [15] E. Ben-Jacob, I. Cohen, O. Shochet, I. Aranson, H. Levine, and L. Tsimiring, *Nature* **373**, 566 (1995).  
 [16] E. Ben-Jacob, I. Cohen, O. Shochet, A. Tenenbaum, A. Czirók, and T. Vicsek, *Phys. Rev. Lett.* **75**, 2899 (1995).  
 [17] W.W. Mullins and R.F. Sekerka, *J. Appl. Phys.* **34**, 323 (1963).  
 [18] T. Vicsek, *Fractal Growth Phenomena* (World Scientific, Singapore, 1989).  
 [19] *Encyclopaedia Cinematographica: Microbiology*, edited by G. Wolf (Institut für den Wissenschaftlichen Film, Göttingen, 1967).  
 [20] Inheritable geometrical property, transferable by a single bacterium. This terminology was suggested by D. Gutnick (private communication).  
 [21] T.A. Witten and L.M. Sander, *Phys. Rev. Lett.* **47**, 1400 (1981).  
 [22] M. Eden, in *Proceedings of the Fourth Berkeley Symposium on Mathematical Statistics and Probability* (University of California Press, Berkeley, 1961), Vol. 4.  
 [23] D. Kessler and H. Levine, *Phys. Rev. E* **48**, 4801 (1993).  
 [24] Y. Tu and J. Toner, *Phys. Rev. Lett.* **75**, 4326 (1995).  
 [25] Y.L. Duparcmeur, H. Herrmann, and J.P. Troadec, *J. Phys (France) I* **5**, 1119 (1995).  
 [26] J. Hemmingsson, *J. Phys. A* **28**, 4245 (1995).  
 [27] T. Vicsek, A. Czirók, E. Ben-Jacob, I. Cohen, and O. Shochet, *Phys. Rev. Lett.* **75**, 1226 (1995).  
 [28] P.G. de Gennes, *The Physics of Liquid Crystals* (Clarendon Press, Oxford, 1974).  
 [29] Z. Csahók and T. Vicsek, *Phys. Rev. E* **52**, 5297 (1995).  
 [30] H.E. Stanley, *Introduction to Phase Transitions and Critical Phenomena* (Oxford University Press, Oxford, 1971).  
 [31] S.K. Ma, *Statistical Mechanics* (World Scientific, Singapore, 1985); *Modern Theory of Critical Phenomena* (Benjamin, New York, 1976).  
 [32] E. Ben-Jacob, I. Cohen, and A. Czirók (unpublished).  
 [33] *Biology of the Chemotactic Response*, edited by J. M. Lackie (Cambridge Univ. Press, Cambridge, 1981).  
 [34] H.C. Berg and E.M. Purcell, *Biophys. J.* **20**, 193 (1977).  
 [35] R. Belas, *ASM News* **58**, 15 (1992).  
 [36] S.J. Stahl, K.R. Stewart, and F.D. Williams, *J. Bacteriol.* **154**, 939 (1983).